How to cite: *Angew. Chem. Int. Ed.* **2021**, *60*, 391 – 398
International Edition: doi.org/10.1002/anie.202010815
German Edition: doi.org/10.1002/ange.202010815

Single-Atom Catalysts

Economizing on Precious Metals in Three-Way Catalysts: Thermally Stable and Highly Active Single-Atom Rhodium on Ceria for NO Abatement under Dry and Industrially Relevant Conditions**

Konstantin Khivantsev, Carlos Garcia Vargas, Jinshu Tian, Libor Kovarik, Nicholas R. Jaegers, Janos Szanyi,* and Yong Wang**

Abstract: *We show for the first time that atomically dispersed Rh cations on ceria, prepared by a high-temperature atom-trapping synthesis, are the active species for the (CO + NO) reaction. This provides a direct link with the organometallic homogeneous Rh^I complexes capable of catalyzing the dry (CO + NO) reaction. The thermally stable Rh cations in 0.1 wt % Rh_1/CeO_2 achieve full NO conversion with a turn-over-frequency (TOF) of around 330 h^{-1} per Rh atom at 120 °C. Under dry conditions, the main product above 100 °C is N_2 with N_2O being the minor product. The presence of water promotes low-temperature activity of 0.1 wt % Rh_1/CeO_2. In the wet stream, ammonia and nitrogen are the main products above 120 °C. The uniformity of Rh ions on the support, allows us to detect the intermediates of (CO + NO) reaction via IR measurements on Rh cations on zeolite and ceria. We also show that NH_3 formation correlates with the water gas shift (WGS) activity of the material and detect the formation of Rh hydride species spectroscopically.*

Introduction

Improving air quality is one of the biggest challenges in the modern post-industrial society.[1,2] The worst "offenders" contributing to air pollution are NOx and CO emissions from vehicles/engines. Various technological advances have allowed to decrease the NO emissions from vehicles significantly relying on so-called "three-way-catalysts (TWC)" and, more recently, selectively catalytic reduction technology (SCR).[1,3–7,9–11,32]

TWC is widely used in a multitude of trucks, passenger cars, motorcycles, lawnmowers and such.[1,3–7] Various industrial formulations exist with Pd and Rh being the main components supported on materials with oxygen storage capacity, such as ceria, ceria-zirconia and others. TWCs become active at temperatures above 200 °C and show impressive performance under these conditions. Industrial and known formulations contain loadings of Rh up to > 0.5 wt % typically with a smear of rhodium species present on the surface—from nanoparticles to small clusters to isolated atoms.[3–7,32] Because of the lack of well-defined uniform materials, the true nature of catalytically active sites remains debated and largely unknown. Furthermore, there remains a formidable "150 °C degree challenge", set forth by the US DOE to allow for the conversion of 90 % of emissions at 150 °C.[8] Moreover, another challenge lies in the high prices of Pd and Rh, especially rhodium with price for ounce reaching about 10 000 USD recently.[10] This means that materials with lower loadings of Rh with comparable activities for NOx conversion are needed. In our study, we utilize the Rh/ceria materials prepared via high-temperature activation (*atom-trapping, AT*) by calcining Rh precursor with the pure ceria nanoparticles at 800 °C[12–14] to tackle these challenges simultaneously by: 1). Producing uniform single-atom Rh^I-containing ceria materials 2). Showing that uniform rhodium atoms are stable and highly catalytically active for TWC 3). Providing mechanistic insight into the (CO + NO) reaction using infrared and kinetic (catalytic) data and 4). Producing materials with 100 % atom economy of Rh (0.1 wt %) with excellent performance and selectivity.

Results and Discussion

We started by first synthesizing 0.5 wt % Rh/Ceria material via the previously developed atom-trapping method.[12–14] The benefits of using this method for the synthesis of atomically dispersed materials/catalysts have been previously established.[12–14] After 800 °C degree calcination in air, the as-prepared material shows significantly higher surface area (for both 0.5 and 0.1 wt % Rh loadings, Table S1) than bare ceria support calcined at this temperature, indicating that transition metal cations (Rh) can stabilize ceria nanoparticles against sintering. This finding is in agreement with our recent report in which we observed the similar stabilizing effect for Pt, Pd and Ru cations prepared on ceria via atom trapping at 800 °C.[39] The synthesized Rh catalysts contain no visible Rh/

[*] Dr. K. Khivantsev, C. G. Vargas, Dr. J. Tian, Dr. L. Kovarik, Dr. N. R. Jaegers, Dr. J. Szanyi, Dr. Y. Wang
Institute for Integrated Catalysis, Pacific Northwest National Laboratory
Richland, WA, 99352 (USA)
E-mail: Konstantin.Khivantsev@pnnl.gov
Janos.Szanyi@pnnl.gov
Yong.Wang@pnnl.gov
C. G. Vargas, Dr. N. R. Jaegers, Dr. Y. Wang
Voiland School of Chemical Engineering and Bioengineering, Washington State University
Pullman, WA, 99163 (USA)

[**] A previous version of this manuscript has been deposited on a preprint server (https://doi.org/10.26434/chemrxiv.12086004.v1).
Supporting information and the ORCID identification number(s) for the author(s) of this article can be found under: https://doi.org/10.1002/anie.202010815.

RhOx nanoparticles as evidenced by high-resolution HAADF-STEM images, EDS mapping as well as CO-FTIR data (Figures 1a,b and Figures S1, S2). As shown in Figure 1b, no metallic Rh signatures could be established and the ≈ 2083 and $\approx 2017\ cm^{-1}$ doublets observed in the FTIR spectra during CO adsorption correspond to CO stretching frequencies of symmetric and asymmetric CO stretches in the di-carbonyl $Rh(CO)_2$ complexes.[15,16] The presence of at least three distinct $Rh^I(CO)_2$ species with corresponding doublets at (2093; 2029), (2083; 2017) and (2068; 1999) cm^{-1} could be observed which suggests that Rh speciation is not entirely uniform and at least 3 different local environments (binding sites) exist on the surface of ceria particles for Rh^I ion at this loading: these Rh^I ions bind CO producing distinct $Rh^I(CO)_2$ complexes that can be distinguished with infra-red: DRIFTS is particularly suitable.[15] The fact that the CO stretches in all these ceria supported Rh^I ions lie below the CO value of the gas-phase CO, means that they belong to the class of classical carbonyl complexes, as opposed to non-classical supported M carbonyl complexes;[16,34] the formation of d^8 square-planar complexes of $2O_{support}$-$Rh^I(CO)_2$ with support oxygens as covalently bound ligands strongly suggests that the binding of Rh to the oxygens of ceria is predominantly covalent which is well-established in the supported Rh^I literature.[15,28,40,41]

We then tested the 0.5 wt% Rh/CeO_2 for (CO + NO) reaction under dry conditions (Figure 2A). The GHSV correspond to 150 $L\,g^{-1}\,h^{-1}$ which is especially relevant under real engine conditions.[8] More specifically, we observed it to be competent catalysts for the two reactions occurring [Eq (1) and (2)]:

$$CO + NO \rightarrow CO_2 + {}^1/_2\ N_2 \quad (1)$$

$$CO + 2NO \rightarrow CO_2 + N_2O \quad (2)$$

Light-off starts above 70 °C, and complete NO conversion is achieved at 100 °C. Significant amounts of N_2O byproduct are produced, with maximum N_2O concentration reaching 230 ppm and almost 95% selectivity at 120 °C (Figure 2B) with conversion profiles shown in Figures S3,S4). It is obvious that single Rh^I ions catalyze NO conversion to N_2O and N_2.

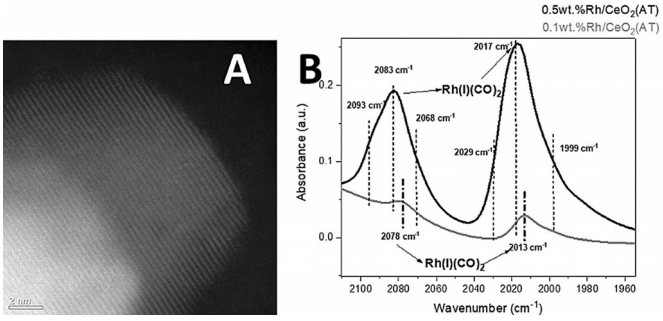

Figure 1. A) HAADF-STEM image of 0.5 wt% Rh/CeO_2 prepared through atom trapping. B) In-situ DRIFTS spectra during CO flow at 125 °C (saturation coverage) for 0.5 and 0.1 wt% Rh/CeO_2 prepared through atom trapping. Note that 0.5 and 0.1 wt% Rh/ceria spectra are shown as is (relative intensities of the CO bands cannot be compared directly to provide quantitative information, the information extracted is qualitative.

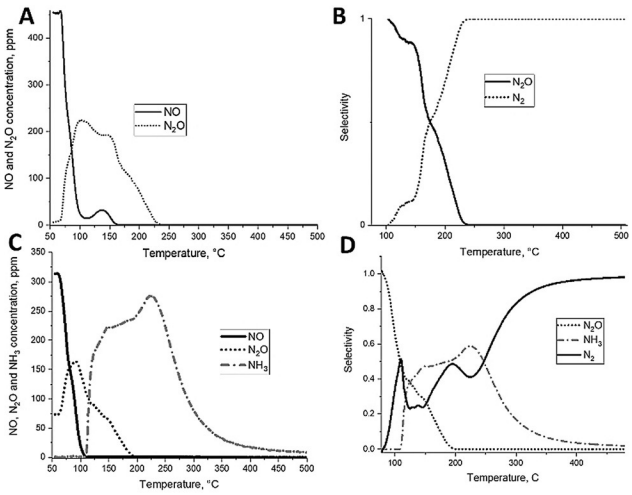

Figure 2. A) Gas concentration versus temperature for dry (NO + CO) reaction. Conditions: 120 mg catalyst 0.5 wt% Rh/CeO_2. Total flow 300 $mL\,min^{-1}$. Concentrations: 460 ppm NO, 1750 ppm CO, balanced with N_2. GHSV $\approx 150\ L\,g^{-1}\,h^{-1}$, ramp rate 2 $K\,min^{-1}$. B) Selectivity versus temperature profile for products of dry (NO + CO) reaction (conditions specified in (A)). C) Gas concentration versus temperature for wet (NO + CO) reaction. Conditions: 120 mg catalyst 0.5 wt% Rh/CeO_2. Total flow 300 $mL\,min^{-1}$. Concentrations: 460 ppm NO, 1750 ppm CO, approximately 2.6% H_2O, balanced with N_2. GHSV $\approx 150\ L\,g^{-1}\,h^{-1}$, ramp rate 2 $K\,min^{-1}$. D) Selectivity versus temperature profile for products of wet (NO + CO) reaction (conditions specified in (C)).

The observed high reactivity of single Rh^I ions in the NO + CO reaction may seem surprising considering the extensive prior work over Rh single crystals and particles.[35–37] It has been shown that for the NO + CO reaction to occur, extended Rh surfaces were required for the dissociation of adsorbed NO molecules and the re-combination of adsorbed N atoms to form N_2. The role of CO was believed to remove adsorbed O atoms originating from the dissociation of NO. The reaction on reduced Rh surfaces is known to proceed with the formation of isocyanate -NCO species. The situation in the case of ionic Rh^I, however, is fundamentally different and likely follows the progression of the NO + CO reaction on a completely different reaction path. First, Rh is present in (1+) oxidation state, in contrast to (0) valence state in single crystals and particles, which modifies the strength and nature of the interaction between adsorbates and the metal center. Second, ionic Rh^I is part of the extended surface of a reducible oxide (CeO_2) that can be an active component. The interaction between NO and CeO_2 can result in the formation of hyponitrites (*as detailed below*), which already contain the N–N bond necessary for N_2 formation.[17–22,38] It is also very likely that both hyponitrites and CO adsorb onto the ionic Rh centers and the reaction between these two adsorbed species takes place while the Rh ion undergoes a (3+) to (1+) redox cycle. This latter reaction path has been observed for the NO + CO reaction over organometallic d^8 Rh^I, Ir^I, Pd^{II} complexes in non-aqueous solution (although among them Pd^{II} gets easily reduced to metallic inactive Pd).[17–22] Those complexes are known to catalyze reaction between NO and CO with the formation of N_2O and more rarely N_2 at

temperatures above 50 °C (however, instability of organometallic complexes at temperatures above 100 °C precludes their activity measurements above ≈100 °C). More specifically, Johnson et al. were the first[17] to demonstrate that $Ir^{I}L_2(NO)_2$ (where ligand L can be PPh_3, for example) in organic solution *stoichiometrically* reacts with CO producing CO_2, N_2O, and the $[IrL_2(CO)_3]^{+1}$ complex. The iridium(I) product can be converted back to $[IrL_2(NO)_2]^{+1}$ under NO pressure with the production of CO_2 and N_2O, thereby closing the cycle. Mechanistic studies[18,19] on analogous Rh and Ir d^8 complexes suggested a monomolecular route. Furthermore, a complete catalytic cycle was proposed for this (CO + NO) reaction[20] using ethanolic $RhCl_3$: the authors concluded that Rh^{III} is not active whereas the formation of $Rh^{I}(CO)_2$ species was a prerequisite for the onset of catalysis under a NO/CO atmosphere. Organometallic complexes, however, demonstrate slow conversion over time with low TOF.[17–22] We suggest that the reaction on the supported Rh^{I}/Ceria system proceeds through the initial formation of $Rh^{I}(NO)_2$ complexes, previously extensively characterized for $Rh^{I}(CO)_2$ and $Rh^{I}(NO)_2$ zeolite supported single atom catalysts.[15,17–21] This route is known for $Rh^{I}(CO)_2$ well-defined complex in zeolites (Figures S11,S12); see further discussion in the text regarding the contrasting Rh^{I}/Zeolite and Rh^{I}/Ceria reactivity with NO based on FTIR measurements. NO chemisorbed on the Rh^{I} center has a fluxional character: due to the ability to shuffle between linear and bent binding, NO molecules can attain a formal +1 (linear) and −1 (bent) charge forming Rh^{I}-$(NO)^{\delta+}(NO)^{\delta-}$ attached to 1 Rh center. Then these NO molecules then couple to form a $Rh^{III}(N_2O_2)$ hyponitrite intermediate from which, with participation of coordinated CO, CO_2 and N_2O then evolve [Eq (3) and (4)]:

$$Rh^{I} + 2NO \rightarrow Rh^{I}(NO)_2 \rightarrow Rh^{I}(NO)^{\delta+}(NO)^{\delta-} \quad (3)$$

$$Rh^{I}(NO)^{\delta+}(NO)^{\delta-} \rightarrow Rh^{III}(N_2O_2) + CO \rightarrow Rh^{III}(CO)(N_2O_2) \rightarrow Rh^{I} + N_2O + CO_2 \quad (4)$$

Preliminary DFT calculations which are underway in our group confirm the favorability of this route.

Rh^{I} ions in 0.5 wt % Rh/Ceria sample are more active than the organometallic complexes (TOF of ≈65 h^{-1} per rhodium basis at 100 °C, approximately 50–100 times more active than organometallic samples[17–22]). Note, that N_2O (laughing gas)[1] forms at low temperature: N_2O amount decreases significantly above 200 °C. Under real engine conditions, water is always present in the engine gas stream, so we tested the activity of this sample in the presence of ≈3 % water vapor (≈30000 ppm). The light-off curve and the corresponding selectivities are summarized in Figure 2c,d. In this case, significant activity is observed already above 50 °C, thus, water promotes low-temperature reactivity of CO + NO. From 50 to 110 °C N_2 and N_2O form (full gas and conversion profiles are presented in Figures S5,S6,S7). Above 100 °C full conversion of NO is achieved; at above 105 °C, a new product appears ammonia (NH_3) in significant amounts, with selectivity to ammonia reaching over ≈50–60 % at temperatures from 150 to 250 °C. N_2O is not produced at temperatures above 200 °C. The production of ammonia during this reaction is beneficial because the produced ammonia can be used for downstream passive SCR technology which does not require sacrificial source of ammonia (urea).[23] Why does water promote the formation of N_2O at lower temperatures than under dry conditions? It can be explained with the following sequence of reactions that we suggest: $Rh^{III}(N_2O_2)$ hyponitrite intermediate is hydrolyzed by H_2O (or by mobile protons present on the surface of ceria in the presence of water) with the formation of hyponitric acid which is unstable at above room temperature and easily decomposes to N_2O and H_2O [Eq (5) and (6)]:

$$Rh^{III}(N_2O_2) + 2H_2O \rightarrow Rh^{III}(OH)_2 + H_2N_2O_2 \quad (5)$$

$$H_2N_2O_2 \rightarrow H_2O + N_2O \quad (6)$$

Under dry conditions $Rh^{III}(N_2O_2)$ can only be reduced directly by CO.[20,21] In the case of wet gas stream, water (or mobile protons formed on the surface from water) facilitates the hydrolysis of the Rh^{III} hyponitrite intermediate. Consequently, CO reacts with Rh^{III} hydroxo complex to form carboxyl Rh^{III} complex[24] from which CO_2 and water evolve and restore the initial Rh^{I} site [Eq (7)]:

$$Rh^{III}(OH)_2 + CO \rightarrow Rh^{III}(OH)_2(CO) \rightarrow Rh^{III}(COOH)(OH) \rightarrow \rightarrow Rh^{I}(H)(OH) + CO_2 \rightarrow Rh^{I} + H_2O + CO_2 \quad (7)$$

Alternatively, CO can be oxidized to carbonate species through a nucleophilic attack of OH^- species [Eq (8)]:

$$Rh^{III}(OH)_2(CO) \rightarrow Rh(H_2CO_3) \rightarrow Rh^{I} + H_2O + CO_2 \quad (8)$$

The suggested mechanistic steps warrant further investigation with the aid of DFT calculations which are underway in our group. Ammonia formation is certainly peculiar. We clarify the reason for its formation unambiguously vide infra but we already can see the hints for the origin of such reactivity in this case. Figure S5 contains the data showing simultaneous CO and NO conversion vs. temperature under wet conditions. It becomes obvious that CO gets consumed not only by NO but by some other process occurring above ≈110 °C. Figure S6 contains the CO and H_2O concentration vs. temperature data, and from those data the explanation arises that CO is consumed by water with the water-gas-shift reactivity: $CO + H_2O \rightarrow CO_2 + H_2$. Small-metal ensembles and probably single metal ions were shown to be active species for this reaction, although the topic remains controversial.[25,26] Thus, Rh species on the surface of ceria catalyze WGS and hydrogen from the WGS is used to hydrogenate NO into NH_3 (this aspect is discussed vide infra). We further clarify mechanistic aspects of it below on the basis of 0.1 wt % Rh/Ceria samples (vide infra).

Understanding the reaction mechanism and trapping the reaction intermediates is not a trivial task in heterogeneous or homogeneous catalysis.[42] Very few well-defined systems exist on which the mechanism of any catalytic reaction could be clarified. For example, in the original studies of the catalytic reaction between (CO + NO) on well-defined organometallic

Rh, Ir and Pt complexes no intermediates have been trapped and the plausible reaction steps have been suggested on the basis of indirect kinetic measurements[20,21] for this homogeneous catalytic reaction. Rh^{I}, Ir^{I}, Ni^{II} d^8 ions in zeolites have been known to catalyze ethylene di- and polymerization and extensively studied for over 50 years. Yet only recently the first clear evidence of intermediate steps involving the oxidative addition of ethylene C–H bonds with the formation of metal vinyl hydride has been revealed and sequential steps involved in this process were observed spectroscopically[20] with FTIR. Having said this, we turned to FTIR to help us clarify the observed reactivity of 0.5 wt% $Rh^{I}(CO)_2$/ceria samples and compared them with well-defined 0.5 wt% $Rh^{I}(CO)_2$ samples anchored in the H-form of FAU zeolite with Si/Al ratio ≈15. Figure S11 shows the well-defined nature of symmetric and asymmetric dicarbonyl stretches of $Rh^{I}(CO)_2$ species anchored in zeolite: they are located on average much higher (by almost 40 cm^{-1}) than those of Rh^{I}/Ceria due to significantly more electropositive nature of a metal fragment on zeolite than on other support, the recently highlighted phenomenon that we have discussed before.[34] The bands are also much sharper due to the more uniform nature of grafting sites in zeolite than on ceria. $Rh^{I}(CO)_2$/FAU easily reacts with NO to form a well-defined $Rh^{I}(NO)_2$ complex with NO symmetric and asymmetric stretches at 1855 and 1779 cm^{-1} correspondingly (Figure S11). The reaction in the presence of ≈2 torr CO and 2 torr NO mixture in the infrared cell even at 200 °C leads to no evolution of products (Figure S12). Thus, Rh^{I} complexes on zeolite are unreactive.

For $Rh^{I}(CO)_2/CeO_2$ sample comparison of the spectrum before and after reaction (introduction of ≈0.3 torr NO) at 60 °C for 5 minutes (Figure S13) indicates the decrease of CO bands—simultaneously, gas-phase N_2O (we show it is indeed gas-phase N_2O in Figure S14) forms. Concurrently, a new N-O stretch arises at ≈1896 cm^{-1}: this can only belong to NO adsorbed on Rh^{III} ions because NO adsorbed on Rh^{I} in zeolite show up below 1850 cm^{-1}. The bands between 1100 and 1000 cm^{-1} belong to hyponitrites.[43] These results are of importance: first of all, they confirm that NO reacts with $Rh^{I}(CO)_2$ with the formation of N_2O and Rh^{III} complex. The catalytic cycling of Rh^{I} and Rh^{III} is the cornerstone of the mechanism that we suggested[20,21] and is directly confirmed by the experimental data. Hyponitrite formation is also observed consistent with coupling of two NO molecules proposed in the literature for organometallic complexes. N_2O and Rh^{III} spectroscopic signatures grow while CO ligands react and disappear (see also sequential spectra in Figure S15, S16 for lower temperatures). Another important finding is the clearly higher reactivity of the $Rh^{I}(CO)_2$ complexes located at lower wavenumbers compared to the $Rh^{I}(CO)_2$ complexes located at higher wavenumbers for Rh^{I}/CeO_2 sample as shown in Figure S13: lower lying pairs of symmetric and asymmetric CO bands of $Rh^{I}(CO)_2$ on ceria show significantly higher drop in intensity upon reaction with NO. This is fully consistent with much higher TOF per Rh basis observed for (CO + NO) reaction on 0.1 wt% Rh/CeO_2 sample vs. 0.5 wt% Rh/CeO_2 sample (see discussion in the text below), with less electropositive nature of Rh in 0.1 wt% Rh/CeO_2 sample inferred from Figure 1 B. Thus, we can now explain the lack of reactivity of Rh^{I}/FAU even at high temperatures: this reaction requires Rh to be significantly less electropositive than Rh^{I} in zeolites. It is important to note that on Rh^{I}/CeO_2 we do not observe the formation of $Rh(NO)_2$ species as an intermediate: we suggest the reason for this is as soon as it forms, it immediately converts to hyponitrites and products of this reaction. Our preliminary DFT data confirm the ease of $Rh^{III}(N_2O_2)$ formation from $Rh^{I}(NO)_2$ on ceria: this is in contrast to zeolites, where $Rh^{I}(NO)_2$ is stable and does not convert to $Rh^{III}(N_2O_2)$ and N_2O even at elevated temperatures.

Another important conclusion for the FTIR data is that during CO + NO reaction on single rhodium ions the mechanism is different from what is well-known for supported Rh nanoparticles.[44] In the case of Rh (Pt and Pd) nanoparticles the reaction proceeds through NO dissociation to N and O on the extended metal surfaces with the following N and CO coupling to form isocyanate (NCO) species which are proven to be intermediates of (CO + NO) reaction on metal surfaces. Indeed, when we in situ reduced Rh^{I}/CeO_2 with H_2 at 700 °C in the FTIR cell to form metallic nanoparticles, and then studied CO + NO reaction, we observed the typical CO bands on metallic surface and very clear formation of isocyanate species at temperatures only around 200 °C (Figure S18). We additionally emphasize that when we reduce Rh/ceria at 700 °C in hydrogen and test for (NO + CO) reaction we observe basically very little (< 5% conversion of NO) reactivity at 120 °C, whereas single atom Rh/ceria materials show high reactivity. This confirms the lack of reactivity of metal nanoparticles in the low-temperature TWC regime when compared with cationic Rh. Our FTIR results also highlight a different mechanism of (CO + NO) reaction on single positively charged Rh atoms which cycle between +1 and +3 oxidation states as suggested in our mechanistic schemes Equations 3–9 and further confirmed by the FTIR data.

We also suggested the possibility of formation of Rh-H species on Rh_1/Ceria: we inferred this on the basis of ammonia formation in the presence of water. Interestingly, Rh_1 ions supported on ceria and zinc oxide were recently reported to be active species for heterogeneous hydroformylation reaction, although no Rh-H intermediates were observed in those studies.[31,45] For homogeneous hydroformylation, the active Rh species are Rh-H species: however, they have never been observed on Rh/ceria or Rh/ZnO catalysts. Not too long ago the first examples of well-defined and well-characterized carbonyl hydride complexes of a transition metal belonging to the platinum group were reported.[28,30,15] Indeed, for Rh/Zeolite it is possible to prepare well-defined $Rh^{III}(CO)H_2$ complexes having undissociated and dissociated hydrogen ligands.[28] Although Rh-H and H-H stretches usually cannot be observed due to their low molar extinction coefficients, due to sharpness of CO bands at sufficiently high Rh loading in zeolite it becomes possible to observe low-intensity Rh-H and H-H stretches. Figure S19 shows $Rh^{III}(CO)H_2$ complexes: CO bands in them are located between symmetric and asymmetric CO stretches of $Rh^{I}(CO)_2$ complexes while Rh-H stretches are above > 2120 cm^{-1}. On

$Rh(CO)_2$ ceria the CO bands are much broader than on Rh(CO)2: for this very reason it would be very difficult to directly observe Rh-H bands if they were to form. However, the CO bands of the candidates should be located between symmetric and asymmetric CO bands of $Rh(CO)_2/CeO_2$. Moreover, Figure S19 shows an experiment in which on Rh/Zeolite $Rh(CO)H_2$ reacted with D_2: Rh-H stretches disappeared, Rh-D stretches appeared in the $\approx$1500–1600 cm^{-1} region due to the isotopic shift; simultaneously due to secondary isotope effect CO band of $Rh(CO)H_2$ shifted lower by $\approx$7 wavenumbers (we also observed similar shift for isostructural $Ir^{III}(CO)H_2$ complexes during exchange with D_2[29]). Moreover, previous method to synthesize $Rh^{III}(CO)H_2$ did not involve direct $Rh^{I}(CO)_2$ reaction with H_2: in that method,[28,30] first, ethylene reacted with $Rh(CO)_2$ to form $Rh(CO)(C_2H_4)$ complex, then H_2 was introduced at 298 K to selectively form $Rh^{III}(CO)H_2$. Direct reaction with H_2 was not observed before on $Rh^{I}(CO)_2$/Zeolite. We now show that it is possible to observe formation of $Rh(CO)H_2$ under direct contact of $Rh(CO)_2$ and H_2 as long as H_2 partial pressure exceeds 2 atmospheres and temperature > 80 °C (Figure S20). To these lines, we reacted $Rh^{I}(CO)_2/CeO_2$ with H_2 at 120 °C. This produced a broad CO band between symmetric and asymmetric CO stretches (the band is between 2040 and 2020 cm^{-1}) of $Rh^{I}(CO)_2/CeO_2$, potentially consistent with the presence of $Rh^{III}(CO)H_2$(Figure S21). Thereafter, we reacted it with D_2 (Figure S21). In this case, similarly to $Rh^{III}(CO)H_2$ on FAU, the CO band in the middle shifted to lower wavenumbers by approximately $\approx$7–8 cm^{-1}, analogous to the zeolite case. Thus we confirm that this CO band belongs to a family of $Rh^{III}(CO)H_2$ complexes and for the first time we show the formation of a Rh-H complex on ceria which explains the reactivity of Rh_1/CeO2 and Rh_1/ZnO in hydroformylation reaction:[31,45] we trapped the catalytically important intermediate in our study and confirmed the feasibility of Rh-H species formation.

The samples with low loading of Rh yield more uniform, well-defined and stable structures (see below) which provide important information about the catalytically active species in this reaction.

Hence, we decreased the Rh loading on ultra-pure ceria to 0.1 wt %. The rational for this was the fact that only the most thermodynamically stable Rh/Ceria structures will be formed upon 800 °C heating at low Rh loading;[12–14] and then with the increase of Rh loading the less thermodynamically stable positions will be filled (after the most stable thermodynamic positions have been filled) which may lead to the lower stability of resulting material. Indeed, FTIR characterization with CO adsorption shows only the presence of majorly 1 particular type of $Rh^{I}(CO)_2$ species on the surface of ceria as opposed to 3 types of $Rh^{I}(CO)_2$ species observed for 0.5 wt % Rh/Ceria sample (Figure 1 B). The corresponding symmetric and asymmetric CO frequencies of $Rh^{I}(CO)_2$ complex in this case are at 2078 and 2013 cm^{-1}, with another smaller component at 2069 and 1999 cm^{-1} (the latter also present in 0.5 wt % Rh/Ceria in significant amounts in Figure 1 B). The FWHM of the bands for this complex is $\approx$10–12 cm^{-1} which is obviously narrower than the major doublet observed for 0.5 wt % Rh/Ceria for which the FWHM $\approx$25 cm^{-1}. Thus, the bonding environment around Rh in 0.1 wt % Rh sample is more uniform and it is grafted predominantly to 1 specific site on the surface of ceria. Moreover, because the CO stretching frequency reflects the electronic state of Rh^{I} ions, the shift to the lower wavenumbers means that Rh in 0.1 wt % Rh/Ceria is on average more electronegative than the majority of Rh in 0.5 wt % Rh/Ceria sample.

We then tested the 0.1 wt % Rh/CeO_2 sample for dry (CO + NO) reaction (Figure 3 a and b). Remarkably, the sample demonstrates complete conversion of NO above 100 °C, with N_2O formed only as a minor species (< 25 ppm) at 75 °C and almost absent at $\approx$120 °C and above. Thus, this isolated Rh^{I} site is very active for this reaction under dry conditions with only minor amount of N_2O formed. CO/NO conversion profiles are summarized in Figures S6. TOF per Rh basis is very high $\approx$330 h^{-1}. We also synthesized the samples with 0.02 wt % and 0.06 wt % Rh loadings: our measurements (Figure S22) confirm that a mononuclear Rh site in involved in the reaction, with reaction rate scaling linearly with Rh loading in the 0–0.1 wt % Rh loading range. Furthermore, CO and NO reaction orders for (CO + NO) reaction summarized in Table S2 show approximately 0 order in CO and NO in the kinetic regime: this is fully consistent with organometallic Rh and Ir complexes which show 0 order in both CO and NO for the reaction,[20,21] drawing parallels to the mechanisms of NO reduction by CO on supported single-atom and organometallic Rh complexes.

Next, we studied the reactivity between (CO + NO) under wet industrial conditions (Figure 3 C,D). The performance of

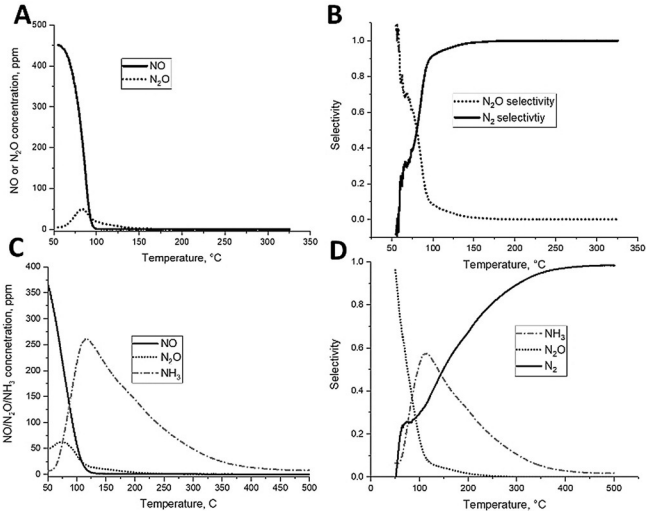

Figure 3. A) Gas concentration versus temperature for dry (NO + CO) reaction. Conditions: 120 mg catalyst 0.1 wt % Rh/CeO_2. Total flow 300 mL min^{-1}. Concentrations: 460 ppm NO, 1750 ppm CO, balanced with N_2. GHSV $\approx$ 150 L g^{-1} h^{-1}, ramp rate 2 K min^{-1}. B) Selectivity versus temperature profile for products of dry (NO + CO) reaction (conditions specified in (A)). C) Gas concentration versus temperature for wet (NO + CO) reaction on 0.1 wt % Rh/CeO_2. Conditions: 120 mg catalyst 0.1 wt % Rh/CeO_2. Total flow 300 mL min^{-1}. Concentrations: 460 ppm NO, 1750 ppm CO, approximately 2.6 % H_2O, balanced with N_2. GHSV $\approx$ 150 L g^{-1} h^{-1}, ramp rate 2 K min^{-1}. D) Selectivity versus temperature profile for products of wet (NO + CO) reaction (conditions specified in (C)).

the low-loaded sample is quite remarkable with full conversion of NO above 120 °C (TOF ≈ 330 h^{-1} at 120 °C). Compared to state-of-the-art novel Rh/ceria-alumina catalysts (≈ 1 wt % Rh)[32] and commercial catalysts TWC[32] containing Rh, which show max TOF ≈ 40–50 h^{-1} under comparable reaction conditions at 150 °C, single uniform Rh^I atoms on ceria are notably active. Moreover, lower amounts of undesirable N_2O byproduct are formed at above 125 °C. Notably, ammonia NH_3 is formed on this material at temperatures above 70 °C with maximum NH_3 selectivity of ≈ 55–60 % at temperatures between 125 and 150 °C.

This sample, containing uniform Rh sites, thus allows us to further confirm the mechanism of NH_3 formation. Plotting NO/CO vs. Temperature profiles as well as CO/H_2O vs. Temperature profiles for wet (NO + CO) reaction (see also discussion vide infra) (Figures S8, S9, S10) provides a very clear visualization of the fact that NH_3 is formed through the path involving hydrogen stored on Rh from water gas shift reaction. Molecular H_2 in the gas phase (at relatively low partial pressures) does not catalyze the formation of ammonia, and thus Rh-H[28,29] rhodium hydride supported species are the important intermediate for NO hydrogenation, which we suggest can be formed through the recently uncovered carboxyl route[24] [Eq (9)]:

$$\text{Rh-OH} + \text{CO} \rightarrow \text{Rh(COOH)} \rightarrow \text{Rh-H} + \text{CO}_2 \quad (9)$$

Hydride formed on rhodium, hydrogenates NO to ammonia at low temperatures. Although the very first supported transition metal carbonyl hydride complex was synthesized and comprehensively characterized for single rhodium(I) atoms in zeolite recently[28] starting with uniform $Rh^I(CO)_2$ zeolite-supported complex, no Rh-H complexes were clearly identified for any other supported Rh material. We have now bridged this gap with Rh/Ceria through isotopic FTIR experiments.

The activity of 0.1 wt % Rh/Ceria for NOx conversion thus rivals that of 0.5 wt % Rh samples with smaller amount of N_2O pollutant formed as a by-product compared to 0.5 wt % Rh/Ceria sample. This directly proves that isolated uniform and more electronegative Rh atoms are the very active catalysts for TWC reaction and NO abatement. Such species are different from multiple species present on 0.5 wt % Rh/Ceria that catalyze, for example, more excessive N_2O formation. In agreement with this suggestion, highly electropositive Rh^I ions in zeolites are inactive for (NO + CO) reaction. TOF for NO abatement at 125 °C is ≈ 330 h^{-1} on the Rh basis for 0.1 wt % Rh/Ceria which is exceptionally high compared to state-of-the-art Rh containing samples.[32] Total NOx conversion is achieved at ≈ 120 °C and above, with only N_2 and ammonia formed as byproducts. Ammonia formation is useful for downstream passive SCR applications.[23] NH_3 formation is possible due to high WGS activity of isolated Rh atoms on ceria and the corresponding formation of rhodium hydride Rh-H species that can hydrogenate NO.

We tested the performance of 0.1 wt % Rh/Ceria and it remains stable for at least 3.5 hours with no sign of deactivation at 150 °C (Figure 4a,b).

We, thereafter, chose to test this sample at 120 °C (the temperature when NO conversion is not complete) for a longer-term stability test during > 7 days. The sample shows excellent stability (Figure S23). However, we note that slow deactivation is observed with time-on-stream: over the space of ≈ 174 hours, the NO level increased from ≈ 10 ppm to ≈ 27 ppm. Simultaneously, slight decline in ammonia formation was observed.

Furthermore, for this sample we performed additional experiments with varying CO levels and their effect on ammonia formation rate (Figure S24): unsurprisingly, at higher CO levels ammonia formation rate increases (due to higher WGS activity under elevated CO pressures).

To assess the effect of unsaturated hydrocarbons, often present in the vehicle exhaust, we carried out experiments on 0.1 wt % Rh/CeO_2 sample in the presence of varying propylene (the most common unsaturated hydrocarbon) levels: from 0 to 360 to ≈ 1100 ppm at 120 °C (Figure S25). We found that propylene does not affect the activity of the sample at low temperature. This is further consistent with lack of reactivity of $Rh^I(CO)_2$ complexes with ethylene during FTIR measurements at 120 °C: even at higher partial pressured of ethylene, when ethylene gas-phase bands can be readily observed in the infrared spectra, no reaction between $Rh^I(CO)_2$ and ethylene occurs on Rh/ceria (Figure S26).

The 0.1 wt % Rh/CeO_2 sample hydrothermally aged at 700 °C in Air/H_2O mix for 10 hours, shows no deterioration in low temperature reactivity (Figure S27), confirming the robustness of materials synthesized via atom trapping at 800 °C.

The high-temperature atom-trapping synthesis is performed by heating at 800 °C (thus, materials are stable at least up to this temperature) and expected to be hydrothermally stable up to 750 °C which is beneficial for industrially relevant materials.[12–14] Moreover, we can further confirm the NH_3 formation rate is coupled to CO consumption based on the CO and NH_3 time-on-stream profiles, showing that steady-state WGS (represented by CO reactivity) activity is achieved simultaneously as steady-state NH_3 production rate is achieved (Figure 4). Since our FTIR data reveal that in the presence of NO, Rh^I oxidation Rh^{III} is possible, this hints at the fact that the excellent WGS activity of Rh_1/CeO_2 at low temperatures is caused by the ability to shuffle between +1 and +3 Rh oxidation states (such shuffle for metal oxides was suggested to be important for WGS activity). Indeed, when we tested the 0.1 wt % Rh/CeO_2 sample for WGS without NO present, we obtained the CO conversion vs. temperature curve that is typical for very active and unpromoted single-atom ceria materials with relatively high metal loadings(such materials have been synthesized for Pt and Au on ceria) (Figure S28).[26] Our 0.1 wt % Rh/ceria sample shows comparable activity than the most active described Pt and Au ceria catalysts with ionic Pt and Au species loaded at higher values,[26] with light-off starting above > 170 °C. We then tested this sample at 120 °C first without NO in the gas-phase (Figure S29), then after adding only ≈ 30 and ≈ 90 ppm NO to the flowing gas stream: remarkably, this led to the increase of CO conversion (while without NO there was no CO

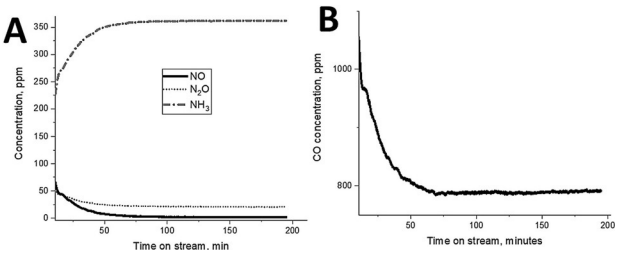

Figure 4. A) Gas concentration for N-containing species (NO, N_2O, NH_3) versus time-on-stream for wet (NO + CO) reaction on 0.1 wt% Rh/CeO_2 at 150 °C. Conditions: 120 mg catalyst 0.1 wt% Rh/CeO_2. Total flow 300 mL min^{-1}. Concentrations: 460 ppm NO, 1750 ppm CO, approximately 2.6% H_2O, balanced with N_2. GHSV ≈ 150 L g^{-1} h^{-1}. B) CO concentration versus time-on-stream simultaneous with conditions as in (A).

conversion), and in the presence of NO the sample became active even at low temperatures.

Conclusion

In summary, we reveal for the first time that Rh^I single atoms dispersed on ceria are the highly active and stable catalytically active species for CO + NO reaction. They are also remarkably active and selective for the wet industrial TWC NO abatement as well, with complete NO abatement above 120 °C. Ammonia formation occurs simultaneously with excellent WGS shift activity of single Rh atoms which suggests the involvement of Rh-H complex as an intermediate in NO hydrogenation.

Thus, we resolve a few outstanding mechanistic issues in the field of TWC catalysis and show a pathway to make novel stable Rh-containing TWC catalysts with 100% precious metal atom economy and excellent low-temperature performance. We also show the direct and previously unrecognized link between the single Rh^I ions on ceria and Rh^I in organometallic complexes in solution: they both catalyze the (CO + NO) reaction with the former being much more active than their organometallic counterparts (> 300–1000 times more active). This adds to the unique repertoire of uniform supported d^8 Rh^I and Ir^I catalysts that demonstrate unique hydrocarbon chemistry recently shown under mild conditions: alkene dimerization,[15] alkene dehydrogenative coupling to dienes,[29,30,33] alkyne/alkyne hydrogenation and hydroformylation.[30,31]

Acknowledgements

K.K., J.T., N.R.J. and J.S.z would like to thank the financial support by Crosscut Lean Exhaust Emissions Reduction Simulations (CLEERS), which is an initiative funded by the U.S. Department of Energy (DOE) Vehicle Technologies Office to support the development of accurate tools for use in the design, calibration, and control of next generation engine/emissions control systems that maximize efficiency while complying with emissions regulations. CG and YW would like to acknowledge the financial support by the U.S. Department of Energy (DOE), Office of Science, Basic Energy Sciences (BES) and Division of Chemical Sciences (grant DE-FG02-05ER15712). Most experiments were conducted in the Environmental Molecular Sciences Laboratory (EMSL), a national scientific user facility sponsored by the Department of Energy's Office of Biological and Environmental Research at Pacific Northwest National Laboratory (PNNL). PNNL is a multi-program national laboratory operated for the DOE by Battelle Memorial Institute under Contract DE-AC06-76RL01830. KK and the authors are grateful to a gifted artist, director and photographer Andrea Giacobbe and Martina Piera for creating cover art for our paper.

Conflict of interest

We are filing for a patent

Keywords: ceria · rhodium · nitric oxide · single atom · three-way catalyst

[1] A. Wang, L. Olsson, *Nat. Catal.* **2019**, *2*, 566–570.
[2] Royal College of Paediatrics and Child Health. Every breath we take-the lifelong impact of air pollution, London, Royal College of Paediatrics and Child Health, **2016**.
[3] M. V. Twigg, *Catal. Today* **2011**, *163*, 33–41.
[4] B. Harrison, A. F. Diwell, C. Hallett, *Platinum Met. Rev.* **1988**, *32*, 73–83.
[5] K. Taylor, *Catal. Rev. Sci. Eng.* **1993**, *35*, 457–481.
[6] P. Granger, V. I. Parvulescu, *Chem. Rev.* **2011**, *111*.
[7] J.-H. Kwak, R. G. Tonkyn, D. H. Kim, J. Szanyi, C. H. F. Peden, *J. Catal.* **2010**, *275*, 187–190.
[8] USDRIVE, Aftertreatment Protocols for Catalyst Characterization and Performance Evaluation, **2015** (https://cleers.org/low-temperature-protocols/).
[9] N. R. Jaegers, J. K. Lai, Y. He, E. Walter, D. A. Dixon, M. Vasiliu, Y. Chen, C. M. Wang, M. Y. Hu, K. T. Mueller, I. E. Wachs, Y. Wang, J. Z. Hu, *Angew. Chem. Int. Ed.* **2019**, *58*, 12609–12616; *Angew. Chem.* **2019**, *131*, 12739–12746.
[10] A. Sykkora, Rhodium prices soar on "demand-driven story", Kitco news, **2020**. https://www.kitco.com/news/2020-01-08/Rhodium-prices-soar-on-demand-driven-story.html.
[11] A. M. Beale, F. Gao, I. Lezcano-Gonzalez, C. H. F. Peden, J. Szanyi, *Chem. Soc. Rev.* **2015**, *44*, 7371–7405.
[12] A. Datye, Y. Wang, *Natl. Sci. Rev.* **2018**, *5*, 630–632.
[13] J. Jones, H. Xiong, A. T. DeLaRiva, E. J. Peterson, H. Pham, S. R. Challa, G. Qi, S. Oh, M. H. Wiebenga, X. I. Pereira Hernandez, Y. Wang, A. K. Datye, *Science* **2016**, *353*, 150–154.
[14] L. Nie, D. Mei, H. Xiong, B. Peng, Z. Ren, X. I. P. Hernandez, A. DeLaRiva, M. Wang, M. H. Engelhard, L. Kovarik, A. K. Datye, Y. Wang, *Science* **2017**, *358*, 1419.
[15] K. Khivantsev, A. Vityuk, H. A. Aleksandrov, G. N. Vayssilov, D. Blom, O. S. Alexeev, M. D. Amiridis, *ACS Catal.* **2017**, *7*, 5965–5982.
[16] H. Miessner, I. Burkhardt, D. Gutschick, A. Zecchina, C. Morterra in *Structure and Reactivity of Surfaces* (Eds.: G. Spoto, C. Morterra, A. Zecchina, G. Costa), Elsevier, Amsterdam, **1989**, pp. 677–684.
[17] B. F. G. Johnson, S. Bhaduri, *J. Chem. Soc. Chem. Commun.* **1973**, 650.
[18] B. L. Haymore, J. A. Ibers, *J. Am. Chem. Soc.* **1974**, *96*, 3325.

[19] S. Bhaduri, B. F. G. Johnson, C. J. Savory, J. A. Segal, R. H. Walter, *J. Chem. Soc. Chem. Commun.* **1974**, 809.
[20] J. Reed, R. Eisenberg, *Science* **1974**, *184*, 568.
[21] C. D. Meyer, R. Eisenberg, *J. Am. Chem. Soc.* **1976**, *98*, 1364.
[22] J. A. Kaduk, T. H. Tulip, J. R. Budge, J. A. Ibers, *J. Mol. Catal.* **1981**, *12*, 239.
[23] V. Y. Prikhodko, J. E. Parks, J. A. Pihl, T. J. Toops, SAE International Journal of Engines 9 (2016-01-0934), 1289 – 1295.
[24] N. C. Nelson, M.-T. Nguyen, V.-A. Glezakou, R. Rousseau, J. Szanyi, *Nat. Catal.* **2019**, https://doi.org/10.1038/s41929-019-0343-2.
[25] K. Ding, A. Gulec, A. M. Johnson, N. M. Schweitzer, G. D. Stucky, L. D. Marks, P. C. Stair, *Science* **2015**, *350*, 189 – 192.
[26] Q. Fu, H. Saltsburg, M. Flytzani-Stephanopoulos, *Science* **2003**, *301*, 935 – 938.
[27] K. Khivantsev, N. R. Jaegers, L. Kovarik, J. C. Hanson, F. F. Tao, Y. Tang, X. Zhang, I. Z. Koleva, H. A. Aleksandrov, G. N. Vayssilov, Y. Wang, F. Gao, J. Szanyi, *Angew. Chem. Int. Ed.* **2018**, *57*, 16672 – 16677; *Angew. Chem.* **2018**, *130*, 16914 – 16919.
[28] K. Khivantsev, A. Vityuk, H. A. Aleksandrov, G. N. Vayssilov, O. S. Alexeev, M. D. Amirdis, *J. Phys. Chem. C* **2015**, *119*, 17166 – 17181.
[29] N. R. Jaegers, K. Khivantsev, L. Kovarik, D. Klas, J. Z. Hu, Y. Wang, J. Szanyi, *Catal. Sci. Technol.* **2019**, *9*, 6570 – 6576.
[30] K. Khivantsev, PhD Thesis, University of South Carolina, **2015**.
[31] R. Lang, T. Li, D. Matsumura, S. Miao, Y. Ren, Y.-T. Cui, Y. Tan, B. Qiao, L. Li, et al. *Angew. Chem. Int. Ed.* **2016**, *55, 16054 – 16058; Angew. Chem.* **2016**, 128, 16288 – 16292; *Angew. Chem.* **2016**, *128*, 16288 – 16292.
[32] H. Jeong, O. Kwon, B.-S. Kim, J. Bae, S. Shin, H.-E. Kim, J. Kim, H. Lee, *Nat. Catal.* **2020**, https://doi.org/10.1038/s41929-020-0427-z.
[33] Y. Gao, T. J. Emge, K. Krogh-Jespersen, A. S. Goldman, *J. Am. Chem. Soc.* **2018**, *140*, 2260 – 2264.
[34] K. Khivantsev, N. R. Jaegers, I. Z. Koleva, H. A. Aleksandrov, L. Kovarik, M. Engelhard, F. Gao, Y. Wang, G. N. Vayssilov, J. Szanyi, *J. Phys. Chem. C* **2020**, *124*, 309 – 321.
[35] R. J. Baird, R. C. Ku, P. Wynblatt, *Surf. Sci.* **1980**, *97*, 346 – 362.
[36] T. W. Root, L. D. Schmidt, G. B. Fisher, *Surf. Sci.* **1983**, *134*, 30 – 45.
[37] S. H. Oh, et al., *J. Catal.* **1986**, *100*, 360 – 376.
[38] S. H. Overbury, et al., *J. Catal.* **1999**, *186*, 296 – 309.
[39] K. Khivantsev, N. R. Jaegers, L. Kovarik, J. Tian, X. Isidro Pereira Hernandez, Y. Wang, J. Szanyi, *Chemrxiv* **2020**, https://doi.org/10.26434/chemrxiv.12692264.
[40] M. J. Hülsey, B. Zhang, Z. Ma, H. Asakura, D. A. Do, W. Chen, T. Tanaka, P. Zhang, Z. Wu, N. Yan, *Nat. Commun.* **2019**, *10*, 1330.
[41] H. F. Van't Bilk, J. B. A. D. Van Zon, T. Huizinga, J. C. Vis, D. C. Konigsberger, R. Prins, *J. Chem. Phys.* **1983**, *87*, 2264.
[42] A. S. Goldman, C. R. Landis, A. Sen, *Angew. Chem. Int. Ed.* **2018**, *57*, 4460; *Angew. Chem.* **2018**, *130*, 4548.
[43] A. M. Wright, T. W. Hayton, *Inorg. Chem.* **2015**, *54*, 9330 – 9341.
[44] A. Srinivasan, C. Depcik, *Catal. Rev. Sci. Eng.* **2010**, *52*, 462 – 493.
[45] J. Amsler, B. B. Sarma, G. Agostini, G. Prieto, P. N. Plessow, F. Studt, *J. Am. Chem. Soc.* **2020**, *142*, 5087 – 5096.

Manuscript received: August 7, 2020
Accepted manuscript online: September 2, 2020
Version of record online: October 28, 2020

